Theoretical description of dissociative 2 scattering in diatomic molecules

K Jänkälä, Ph V Demekhin, S Heinäsmäki, I Haar, R Hentges, A Ehresmann

▶ **To cite this version:**

K Jänkälä, Ph V Demekhin, S Heinäsmäki, I Haar, R Hentges, et al.. Theoretical description of dissociative 2 scattering in diatomic molecules. Journal of Physics B: Atomic, Molecular and Optical Physics, 2010, 43 (6), pp.65104. 10.1088/0953-4075/43/6/065104 . hal-00630008

HAL Id: hal-00630008
https://hal.science/hal-00630008

Submitted on 7 Oct 2011

HAL is a multi-disciplinary open access archive for the deposit and dissemination of scientific research documents, whether they are published or not. The documents may come from teaching and research institutions in France or abroad, or from public or private research centers.

L'archive ouverte pluridisciplinaire **HAL**, est destinée au dépôt et à la diffusion de documents scientifiques de niveau recherche, publiés ou non, émanant des établissements d'enseignement et de recherche français ou étrangers, des laboratoires publics ou privés.

Confidential: not for distribution. Submitted to IOP Publishing for peer review 9 February 2010

Theoretical description of dissociative $\gamma \rightarrow 2\gamma'$ scattering in diatomic molecules

K Jänkälä[1,2], Ph V Demekhin[1], S Heinäsmäki[2], I Haar[1], R Hentges[1] and A Ehresmann[1]

[1]Institute of Physics, University of Kassel, Heinrich-Plett-Straße 40, D-34132 Kassel, Germany

[2]Department of Physical Sciences, University of Oulu, P.O. Box 3000 90014 Oulu, Finland

E-mail: kari.jankala@oulu.fi

Abstract. The paper describes the theoretical formulation of dissociative $\gamma \rightarrow 2\gamma'$ scattering in fixed-in-space and randomly oriented diatomic molecules in the dipole approximation for excitation and $2\gamma'$ production. Based on perturbation theory the double differential cross section and two-photon angular correlation function of the process is derived. The developed theory is applied to study the angular correlation function of the two Lyman-α photons produced via decay of the doubly-excited $Q_2\,^1\Pi_u(1)$ state of the H_2 molecule.

Submitted to: *J. Phys. B: At. Mol. Opt. Phys.*

1. Introduction

Doubly-excited molecular states, where two electrons are promoted from the ground state into initially unoccupied orbitals, usually lie energetically above the first ionization and dissociation thresholds (see, e.g. the reviews [1, 2] and [3]). These states are sometimes called 'superexcited' [4] and may decay either via autoionization or neutral dissociation accompanied by photon emission [1]. Due to the variety of different relaxation pathways, strong couplings with the electronic continua, and fairly small excitation cross sections, these states are generally difficult to study both, experimentally and theoretically [3]. During the last decades, superexcited states have been studied experimentally in diatomic and polyatomic molecules using several different techniques [2], such as ion spectroscopy [5], electron-energy-loss spectroscopy [6], and one fluorescence photon [7] or two fluorescence photon coincidence spectroscopies [8, 9]. Particularly for the latter type of experiments theoretical approaches as scarce [10]. Therefore, in the present paper, the main goal is an extended theoretical description of the two-photon coincident emission from dissociation fragments of one-photon superexcited states in diatomic molecules.

One-photon doubly-excited molecular states in diatomic molecules leading after neutral dissociation to an emission of two photons may be divided in two groups. In the first group, dissociation of a molecular superexcited state results in excited atomic fragments, with one in a metastable state. The decay of the $Q_1\,^1\Pi$ state of H_2 into the H($2p$) and H($2s$) fragments [7] is an example of this type. The radiative decay of the metastable state takes place mainly due to collisional quenching (see, e.g. [11] and references therein). Therefore, the angular correlation between the two emitted photons in this case does not carry precise information on the entangled atomic fragments. In the second group, dissociation of a superexcited state forms two atomic fragments in excited states decaying via dipole transition operator. The $Q_2\,^1\Pi_u(1)$ superexcited state of H_2 dissociating into the H($2p$) and H($2p$) fragments [8] belongs to this second group of processes. Such a two-photon emission process is very interesting, because the two photons carry now detailed information on the structure and de-excitation dynamics of the doubly excited molecular state. The two photons are entangled, since they are emitted from an entangled excited-atom pair, even if the atomic fragments are far from each other. Importance of entanglement of atomic fragments and its impact on correlation in the two photons emission has been pointed out in [10]. Below we focus on the decay of superexcited states within this second group.

The possibility to experimentally detect the two photons in coincidence emitted via the dissociation of superexcited states into two excited fragments were shown in the late 1980's by Arai *et al* [8] in their pioneering experiments. The authors recorded the absorption profile of the $Q_2\,^1\Pi_u(1)$ state of H_2 using the two-photon coincidence technique. The experiment is very demanding mainly due to the requirement of coincidence detection and small excitation cross section. Thus, the technique was unused for more than 25 years. Higher photon flux of the modern synchrotron radiation sources provides more feasible framework for this method, and the task was recently revived by Odagiri *et al* [9] by repeating the original experiment on H_2. Since then, similar photon-photon coincidence experiments have been carried out by the same group also for the homonuclear molecules N_2 [12, 13] and O_2 [14], and the heteronuclear molecule NO [15]. Recently, this group published also the first experimental work devoted to the measurement of the angular correlation function (ACF) of the two photons emitted after the neutral dissociation of the $Q_2\,^1\Pi_u(1)$ state of H_2 [16].

The theoretical description of doubly-excited states in molecules is demanding, and so far mainly carried out for H_2. As an example, Guberman [17] has calculated energies and Bottcher [18] potential energy curves and transition moments for several doubly-excited states in H_2. Calculations of the exciting photon energy dependence of the absorption cross section based on semiclassical approximation were reported in [9, 19]. The full quantum mechanical treatment of the problem is presented by Borges and Bielschowsy in [20]. To the best of our knowledge, so far only one theoretical work has been devoted to the derivation of the ACF of two photons emitted after dissociation of a superexcited molecular state [10]. The two-photon ACF obtained by Miyagi *et al* [10] is based on the second-order correlation function in quantum optics and was

used to study solely H_2. Their approach, based on the analysis of the symmetry of the dissociating doubly-excited state is elegant. However, it is challenging to extend it to take into account different polarizations of the exciting radiation, general molecular states, orientations of a molecule and decays to different spin-orbit components.

In this paper we present a theoretical description of one-photon excitation of doubly excited molecular states, their dissociation into two excited atomic fragments, and the following two-photon emission of diatomic molecules. Our model is based on perturbation theory and can be readily applied to all diatomic molecules. The model allows calculations with variable polarization of the incoming radiation, and polarization sensitivities of the photon counters. The theory is applied to study the ACF of the two Lyman-α photons produced via excitation and decay of the $Q_2\,{}^1\Pi_u(1)$ state of the fixed-in-space and randomly oriented H_2 molecules. The ACF is studied in different cases and compared to the existing theoretical and experimental data. Atomic units are used throughout the paper unless otherwise stated.

2. Theory

In the following section we formulate the double differential cross section for one photon excitation and two photon decay of doubly-excited states of diatomic molecules. We are, thus, interested in the following process:

$$AB + h\nu_i \to (AB)^{**} \to A^* + B^* \to A + B + h\nu_f + h\nu'_f, \tag{1}$$

where the incoming photon $h\nu_i$ excites molecule AB from the initial state to the doubly-excited state $(AB)^{**}$. The state dissociates into the excited atomic fragments A^* and B^*, which emit subsequently two photons proceeding into stable states A and B. Thereby, we assume that the radiative decay is slow compared with the dissociation. It is also assumed, that the doubly-excited resonance is isolated allowing lifetime interference effects to be neglected. A schematic view of the coordinate system used in the calculations is shown in figure 1.

2.1. Wave functions

The molecular wave functions are described in Hund's coupling case (a) [21, 22] by

$$|JM\nu\Omega\rangle = \sqrt{\frac{2J+1}{8\pi^2}}\mathcal{D}^{J*}_{M\Omega}(\omega)|\nu\rangle|\Omega\rangle, \tag{2}$$

where Wigner's rotation matrix $\mathcal{D}^J_{M\Omega}(\omega)$ describes the molecular rotational motion, $|\nu\rangle$ denotes the vibrational wave function, and $|\Omega\rangle$ is the electronic part of the total wave function. Quantum numbers J and M are the total angular momentum of the molecule and its projection on the quantization axis. In Hund's case (a) $\Omega = \Lambda + \Sigma$, where Λ and Σ are projections of the total orbital angular momentum and total spin on the molecular axis. The theory can be directly applied to other Hund's cases by using the basis transformations given elsewhere (see, e.g. [23]). The molecular wave function (2)

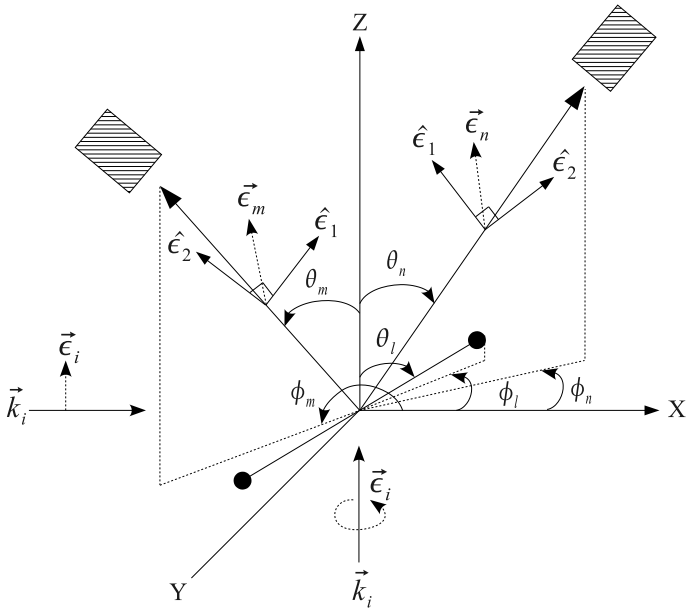

Figure 1. The coordinate system used. Positions of the detectors as well as the molecular orientation are described by polar $\theta \in [0, \pi]$ and azimuth $\phi \in [0, 2\pi]$ angles. The incoming photon propagates along the x- or z-axis depending on the chosen polarization. The polarization vectors of the outgoing photons are described in the basis spanned by spherical unit vectors $\hat{\epsilon}_1$ and $\hat{\epsilon}_2$.

does not describe a defined parity of a molecular state, but due to the closure relation, the use of parity adapted wave functions becomes superfluous.

In the limit of large internuclear fragment separation, the adiabatic electronic wave functions are written as linear combinations of atomic wave functions [24] as

$$|C\Omega\rangle \overset{r\to\infty}{\longrightarrow} \sum_{j_a\Omega_a j_b\Omega_b} M(j_a\Omega_a j_b\Omega_b|C\Omega)|c_a j_a\Omega_a\rangle|c_b j_b\Omega_b\rangle, \tag{3}$$

where j is the total angular momentum of an atomic fragment (a or b) and Ω is its projection on the molecular quantization axis. The atomic quantum numbers $j_a\Omega_a$ and $j_b\Omega_b$ (including their signs) are strictly selected in the sum (3) by the entanglement of the two electronic states of atoms in the overall molecular electronic state $|C\Omega\rangle$, including signs and values of all quantum numbers of the molecular state (i.e. spin S, its projection Σ, orbital angular momentum L and its projection $\Lambda = \Omega - \Sigma$) labeled here by index C. The coefficients $M(j_a\Omega_a j_b\Omega_b|C\Omega)$ are given explicitly via Clebsch-Gordan coefficients in [24].

2.2. Transition matrix elements

We start by defining the transition amplitudes for initial excitation, fragmentation and subsequent two-photon emission by a two-step cascade by

$$\langle \alpha_f; h\nu_m h\nu_n|\mathcal{H}|\alpha_i; h\nu_i\rangle = (8\pi^3\omega_i\omega_n\omega_m)^{1/2} \times$$

$$\sum_{\alpha_m \alpha_n \alpha'_n} \frac{\langle \alpha_f | \vec{\epsilon}_m^{\,*} \cdot T^{(1)} | \alpha_m \rangle \langle \alpha_m | \vec{\epsilon}_n^{\,*} \cdot T^{(1)} | \alpha_n \rangle \langle \alpha_n | H_v | \alpha'_n, r_0 \rangle \langle \alpha'_n, r_0 | \vec{\epsilon}_i \cdot T^{(1)} | \alpha_i, r_0 \rangle}{(E - E_m + i\Gamma_m/2)(E - E_n + i\Gamma_n/2)(E - E_{n'} + i\Gamma_{n'}/2)}, \tag{4}$$

where $\langle \alpha | \vec{\epsilon} \cdot T^{(1)} | \alpha' \rangle$ are the dipole transition matrix elements, $|\alpha\rangle$ denotes general molecular states, and H_v is the Hamiltonian for the nuclear dynamics describing (pre)dissociation [25, 26]. In (4) we have neglected the propagation of atomic fragments between the emission of the first and second photon. The exciting and emitted photons are described using a second-quantized vector potential for the electromagnetic field characterized by the creation and annihilation operators of photons with specific polarization and momentum. In the calculations of the matrix elements, the vector potential is taken in the dipole approximation. The first two terms in the denominator of the transition amplitude (4) are the diagonal matrix elements of the Green's function with the radiative linewidths Γ_n and Γ_m [25, 26, 27]. $\Gamma_{n'}$ is the total decay rate of the superexcited state $|\alpha'_n\rangle$, equal to the sum of its autoionization and (pre)dissociation rates [21, 27] neglecting direct fluorescence deexcitation. Energies E_n and E_m are equal to $E_n \overset{r\to\infty}{\longrightarrow} E_n^{\rm at} + \varepsilon_n^{\rm k}$ and $E_m \overset{r\to\infty}{\longrightarrow} E_m^{\rm at} + \varepsilon_m^{\rm k} + h\nu_n = E_n^{\rm at} + \varepsilon_m^{\rm k}$, where $E^{\rm at}$ and $\varepsilon^{\rm k}$ are the total electronic and kinetic energies of the fragments when $r \to \infty$. E is the total energy of the system equal to $E_i + h\nu_i$.

The double differential cross section is calculated in the lowest order of perturbation theory utilizing the Fermi's golden rule

$$\frac{{\rm d}\sigma^2_{nm}}{{\rm d}\Omega_n {\rm d}\Omega_m} = 2\pi\rho \sum_{\alpha_f} |\langle \alpha_f; h\nu_m h\nu_n | \mathcal{H} | \alpha_i; h\nu_i \rangle|^2 \, \delta(E - E_f^{\rm at} - \varepsilon_f^{\rm k} - h\nu_n - h\nu_m), \tag{5}$$

where ρ is the product of densities of the incoming and outgoing radiation modes [26]. We proceed by inserting the wave functions (2) and matrix elements (4) into (5), and integrating over the kinetic energy of the fragments (see, e.g. [28]). It is assumed, that all symmetry quantum numbers are conserved during the dissociation and that the Franck-Condon approximation is valid on each step of the process. Averaging over the degenerate M_i states and dividing by the incident photon flux we obtain on the energy shell

$$\begin{aligned}\frac{{\rm d}\sigma^2_{nm}}{{\rm d}\Omega_n {\rm d}\Omega_m} = \frac{\alpha^4 \omega_i \omega_n^3 \omega_m^3}{4\pi^2 c^3 \hat{J}_i^2} \chi^{\rm diss} \sum_{M_i J_f M_f \Omega_i \Omega_f} \Bigg| \sum_{J_n J_m M_n M_m \Omega_n \Omega_m} \\ \frac{\langle J_f M_f \Omega_f | \vec{\epsilon}_m^{\,*} \cdot T^{(1)} | J_m M_m \Omega_m \rangle}{E_f^{\rm t} - E_m^{\rm t} + h\nu_m + i\Gamma_m/2} \frac{\langle J_m M_m \Omega_m | \vec{\epsilon}_n^{\,*} \cdot T^{(1)} | J_n M_n \Omega_n \rangle}{E_m^{\rm t} - E_n^{\rm t} + h\nu_n + i\Gamma_n/2} \times \\ \langle \nu_n, r_0 | \nu_i, r_0 \rangle \langle J_n M_n \Omega_n, r_0 | \vec{\epsilon}_i \cdot T^{(1)} | J_i M_i \Omega_i, r_0 \rangle \Big|^2,\end{aligned} \tag{6}$$

where the assumption of a fast homogeneous dissociation yields the branching ratio $\chi^{\rm diss} = 2\pi \left| \langle J_n M_n \Omega_n | H_v | J_n M_n \Omega_n, r_0 \rangle \right|^2 / \Gamma_{n'}$, which is assumed to be the same for all $|J_n M_n \Omega_n\rangle$ states. The Franck-Condon factor for the initial excitation is denoted by $\langle \nu_n, r_0 | \nu_i, r_0 \rangle$, $\alpha = 1/137$ is the fine structure constant, and notation $\hat{x}$ stands for $\sqrt{2x+1}$.

In order to calculate the double differential cross section for randomly oriented molecular samples, the first step consists in the analytical integration over the rotational

parts. Applying (A.1) from the appendix to the dipole transition matrix elements in (6) we obtain

$$\begin{aligned}\frac{\mathrm{d}\sigma^2_{nm}}{\mathrm{d}\Omega_n \mathrm{d}\Omega_m} = \frac{\alpha^4 \omega_i \omega_n^3 \omega_m^3}{4\pi^2 c^3 \hat{J}_i^2} \chi^{\mathrm{diss}} \sum_{M_i J_f M_f \Omega_i \Omega_f} \Bigg| \Gamma^{-1} \sum_{J_n J_m M_n M_m \Omega_n \Omega_m} \sum_{p_i p_n p_m} \sum_{q_i q_n q_m} \\ (-1)^{p_i+p_n+p_m} \epsilon_{-p_i} \epsilon^*_{-p_n} \epsilon^*_{-p_m} \hat{J}_f \hat{J}_m^2 \hat{J}_n^2 \hat{J}_i \times \\ (-1)^{M_f+M_m+M_n-\Omega_f-\Omega_m-\Omega_n} \langle \nu_n, r_0 | \nu_i, r_0 \rangle \times \\ \begin{pmatrix} J_f & 1 & J_m \\ -M_f & p_m & M_m \end{pmatrix} \begin{pmatrix} J_m & 1 & J_n \\ -M_m & p_n & M_n \end{pmatrix} \begin{pmatrix} J_n & 1 & J_i \\ -M_n & p_i & M_i \end{pmatrix} \times \\ \begin{pmatrix} J_f & 1 & J_m \\ -\Omega_f & q_m & \Omega_m \end{pmatrix} \begin{pmatrix} J_m & 1 & J_n \\ -\Omega_m & q_n & \Omega_n \end{pmatrix} \begin{pmatrix} J_n & 1 & J_i \\ -\Omega_n & q_i & \Omega_i \end{pmatrix} \times \\ \langle \Omega_f | T^{(1)}_{q_m} | \Omega_m \rangle \langle \Omega_m | T^{(1)}_{q_n} | \Omega_n \rangle \langle \Omega_n | T^{(1)}_{q_i} | \Omega_i \rangle \Big|^2 . \end{aligned} \tag{7}$$

Index p identifies tensor components in the laboratory coordinates and index q in the molecule fixed frame [22]. Components ϵ_{-p} describe polarizations as well as directions of the incoming and outcoming photons and

$$\Gamma = (E^{\mathrm{t}}_f - E^{\mathrm{t}}_m + h\nu_m + i\Gamma_m/2)(E^{\mathrm{t}}_m - E^{\mathrm{t}}_n + h\nu_n + i\Gamma_n/2). \tag{8}$$

Summations over all M quantum numbers were carried out analytically by applying (A.2) twice to the sum over M_n and M_m and using the orthogonality of the $3j$ symbols in summations over M_f and M_i. We obtain then the result

$$\begin{aligned}\frac{\mathrm{d}\sigma^2_{nm}}{\mathrm{d}\Omega_n \mathrm{d}\Omega_m} = \frac{\alpha^4 \omega_i \omega_n^3 \omega_m^3}{4\pi^2 c^3} \chi^{\mathrm{diss}} \sum_{J_f \Omega_i \Omega_f} \sum_{K' Q'} \hat{J}_f^2 \hat{K}'^2 \Bigg| \Gamma^{-1} \sum_K F^{Q'}_{KK'} \sum_{J_n J_m \Omega_n \Omega_m} \langle \nu_n, r_0 | \nu_i, r_0 \rangle \times \\ (-1)^{J_f+2J_m+J_n-\Omega_m-\Omega_n} \hat{J}_m^2 \hat{J}_n^2 \begin{Bmatrix} 1 & 1 & K \\ J_i & J_m & J_n \end{Bmatrix} \begin{Bmatrix} 1 & K & K' \\ J_i & J_f & J_m \end{Bmatrix} \times \\ \begin{pmatrix} J_f & 1 & J_m \\ -\Omega_f & \Omega_f - \Omega_m & \Omega_m \end{pmatrix} \begin{pmatrix} J_m & 1 & J_n \\ -\Omega_m & \Omega_m - \Omega_n & \Omega_n \end{pmatrix} \begin{pmatrix} J_n & 1 & J_i \\ -\Omega_n & \Omega_n - \Omega_i & \Omega_i \end{pmatrix} \times \\ \langle \Omega_f | T^{(1)}_{q_m} | \Omega_m \rangle \langle \Omega_m | T^{(1)}_{q_n} | \Omega_n \rangle \langle \Omega_n | T^{(1)}_{q_i} | \Omega_i \rangle \Big|^2 , \end{aligned} \tag{9}$$

where $q_i = \Omega_n - \Omega_i$, $q_n = \Omega_m - \Omega_n$, $q_m = \Omega_f - \Omega_m$ and the following designation has been used

$$F^{Q'}_{KK'} = \hat{K}^2 \sum_{p_i p_n p_m} (-1)^{p_i+p_n} \epsilon_{-p_i} \epsilon^*_{-p_n} \epsilon^*_{-p_m} \begin{pmatrix} 1 & 1 & K \\ p_i & p_n & -(p_i+p_n) \end{pmatrix} \begin{pmatrix} K & 1 & K' \\ p_i+p_n & p_m & Q' \end{pmatrix} . \tag{10}$$

Tensor $F^{Q'}_{KK'}$ contains all necessary information about polarizations and directions of the incoming and outcoming photons in the laboratory frame, and is the two-photon generalization of the function F_K introduced in [25] for the one-photon decay. One should note that after summing over indices M_i and M_f, summation over index K must be performed coherently, and over K' incoherently, which differs from the one-photon case where only the incoherent summation is required [25]. This leads to interference between $F^{Q'}_{KK'}$ components with different K.

The radiative decay widths of excited atomic fragments are usually much smaller than experimental fluorescence detection resolution. This requires an integration of the double differential cross section (7) over the fluorescent photon energies $h\nu_n$ and $h\nu_m$. This integration will eliminate the Γ^{-1} factor (8) from (7) yielding the constant $4\pi^2/(\Gamma_n\Gamma_m)$ prefactor in the integrated double differential cross section. This, however, will not change the final result for the ACF discussed below.

When only the shape of the two-photon emission pattern (i.e. ACF) is of interest and the J dependence of the vibronic molecular wave functions can be neglected, the double differential cross section can be approximated by considering only the electronic parts of the molecular wave function. Under these assumptions the double differential cross section (9) provides the complete information on the ACF, which reads

$$\frac{\mathrm{d}\sigma^2_{nm}}{\mathrm{d}\Omega_n \mathrm{d}\Omega_m} \propto f(\theta_n,\phi_n,\theta_m,\phi_m) = \int \mathrm{d}\omega_l \sum_{\Omega_i\Omega_f} | \sum_{\Omega_n\Omega_m} \sum_{p_i p_n p_m} (-1)^{p_i+p_n+p_m} \epsilon_{-p_i}\epsilon^*_{-p_n}\epsilon^*_{-p_m} \times$$
$$\mathcal{D}^{(1)}_{p_i q_i}(\omega_l)\mathcal{D}^{(1)}_{p_n q_n}(\omega_l)\mathcal{D}^{(1)}_{p_m q_m}(\omega_l)\langle\Omega_f|T^{(1)}_{q_m}|\Omega_m\rangle\langle\Omega_m|T^{(1)}_{q_n}|\Omega_n\rangle\langle\Omega_n|T^{(1)}_{q_i}|\Omega_i\rangle|^2, \quad (11)$$

where $\omega_l = (\phi_l, \theta_l, 0)$ specifies the orientation of the internuclear axis with respect to the laboratory coordinates (see, figure 1). Equation (11) is the two-photon generalization of the original one-photon emission result by van Brunt and Zare [29] (see also [25]).

2.3. Description of photons

An explicit expression for of the polarization dependent two-photon ACF can be calculated by introducing the general polarization vector

$$\vec{\epsilon} = \cos\xi\hat{\epsilon}_1 + \sin\xi \mathrm{e}^{i\delta}\hat{\epsilon}_2 \quad (12)$$

in the detector frame [30] (see, figure 1). Terms ξ and δ parametrize the polarization response of the detector in such a way that ξ is the angle between the polarization vector and $\hat{\epsilon}_1$, and δ is the phase between $\hat{\epsilon}_1$ and $\hat{\epsilon}_2$ shown in figure 1. Choosing $\delta = 0$ denotes detector sensitivity to linear polarization with polarization angle ξ, and $\delta = \pm\pi/2$ with $\xi = \pi/4$ gives the right- or left-handed circular polarization. Integration over the polarization sensitivities ξ and δ corresponds to polarization insensitive detector. Basis vectors $\hat{\epsilon}_1$ and $\hat{\epsilon}_2$ are the spherical unit vectors

$$\begin{aligned} \hat{\epsilon}_1 &= \cos\theta\cos\phi\hat{x} + \cos\theta\sin\phi\hat{y} - \sin\theta\hat{z}, \\ \hat{\epsilon}_2 &= -\sin\phi\hat{x} + \cos\phi\hat{y} \end{aligned} \quad (13)$$

in the laboratory frame. Introducing the usual definition of the helicity basis vectors

$$\hat{e}_{\pm1} = \mp\frac{1}{\sqrt{2}}(\hat{x} \pm i\hat{y});\ \hat{e}_0 = \hat{z}, \quad (14)$$

polarization vector $\vec{\epsilon}$ can be expressed in the helical basis as

$$\vec{\epsilon} = -\frac{1}{\sqrt{2}}(\cos\xi\cos\theta - i\sin\xi)\mathrm{e}^{-i\phi}\hat{e}_{+1} +$$
$$\frac{1}{\sqrt{2}}(\cos\xi\cos\theta + i\sin\xi)\mathrm{e}^{i\phi}\hat{e}_{-1} - \cos\xi\sin\theta\hat{e}_0. \quad (15)$$

The same equation can be also used to describe the direction and polarization of the incoming radiation.

3. Results and discussion

As a particular example we study the $|^1\Sigma_g\rangle + h\nu_i \to |^1\Sigma_u\rangle + h\nu_m + h\nu_n$ dissociative inelastic scattering via $|Q_2\,^1\Pi_u(1)\rangle$ doubly-excited state in the homonuclear diatomic molecule H_2. We discuss the two-photon ACF for the decays of the $H(2p_0)$ and $H(2p_{\pm1})$ fragments formed via the dissociating $|Q_2\,^1\Pi_u(1)\rangle$ molecular state.

The energy of one-photon excitation cross section of the $|^1\Sigma_g\rangle \to |Q_2\,^1\Pi_u(1)\rangle$ state is about 35 eV and the dipole transition moment has been calculated to be about 0.064 a.u. at $r_0 = 1.4$ a_0 [20], being about three times smaller than in [18]. The complete excitation and two-step decay process in H_2 can be written as

$$|r_0, {}^1\Sigma_g\rangle + h\nu_i \overset{t_0}{\to} |^1\Pi_u\rangle^{**} \overset{t_0\to t_1}{\rightrightarrows} \begin{matrix} |^1\Pi_g\rangle^* \\ |^1\Sigma_g\rangle^* \end{matrix} + h\nu_n \overset{t_1\to t_2}{\to} |^1\Sigma_u\rangle + h\nu_m. \tag{16}$$

The molecule is excited to a dissociative $|r_0, {}^1\Pi_u\rangle^{**}$ state at time t_0. The first photon $h\nu_n$ is emitted at t_1 resulting in a $|^1\Pi_g\rangle^*$ or $|^1\Sigma_g\rangle^*$ intermediate state. Both of these states decay subsequently to the same final state $|^1\Sigma_u\rangle$ via emission of the second photon $h\nu_m$ at time t_2.

3.1. Fixed-in-space H_2 and polarization insensitive detectors

As a first example we study the ACF in the case of fixed-in-space H_2. The molecule is excited by linearly polarized light and the outgoing photons are counted with polarization insensitive detectors. The ACF in the considered case can be most conveniently calculated using equation (11). The coordinate system was chosen so that the incoming photon propagates along the laboratory x-axis and is polarized into the direction of the z-axis, corresponding to vertical polarization in the laboratory frame. The molecular quantization axis coincides with the laboratory y-axis, which corresponds to the geometry used in [10]. In the molecule fixed frame, summation over positive and negative projections of the angular momenta Ω gives four pathways leading to the same final state

$$\Omega_i = 0 \overset{q_i=\pm1}{\longrightarrow} \Omega_n = \pm1 \begin{cases} \overset{q_n=0}{\longrightarrow} \Omega_m = \pm1 \overset{q_m=\mp1}{\longrightarrow} \\ \overset{q_n=\mp1}{\longrightarrow} \Omega_m = 0 \overset{q_m=0}{\longrightarrow} \end{cases} \Omega_f = 0. \tag{17}$$

The ACF was calculated by replacing the molecular wave functions at large internuclear separation by linear combinations of atomic wave functions (3). The atomic dipole transition matrix elements were calculated assuming pure LS-coupling scheme and applying the Wigner-Eckart theorem [31]. As a result the ACF reads

$$f(\theta_n, \phi_n, \theta_m, \phi_m) = \frac{1}{2}|\epsilon_1^n\epsilon_0^m + \epsilon_0^n\epsilon_1^m + \epsilon_{-1}^n\epsilon_0^m + \epsilon_0^n\epsilon_{-1}^m|^2 \times$$
$$|\frac{2}{9}(2\sqrt{2}-3)\langle 1s\|T^{(1)}\|2p\rangle^2\langle {}^1\Pi_u^{\Lambda=|\pm1|}|T^{(1)}_{q_i=|\pm1|}|^1\Sigma_g\rangle|^2, \tag{18}$$

where the first term contains all angular and polarization information of the emitted two photons, and the second term is only a constant factor. In the following, for convenience, ACFs are normalized so that their maxima correspond to unity.

Inserting the vector components of (15) into (18) and integrating over the polarization sensitivities ξ_n, ξ_m, δ_n and δ_m we found that

$$f(\theta_n, \pi/2, \theta_m, 3\pi/2) = \sin^2(\theta_n - \theta_m). \tag{19}$$

Here, choosing $\phi_n = \pi/2$ and $\phi_m = 3\pi/2$ aligns the detectors to opposite sides in plane perpendicular to the direction of propagation of the incoming radiation (i.e. the dipole plane). The ACF (19) is depicted in figure 2. We note that the function in figure 2 coincides with the weighting factor I_{00} for the $\langle T_{00} \rangle$ multipole calculated for two-photon production of electron-impact excited atoms [32].

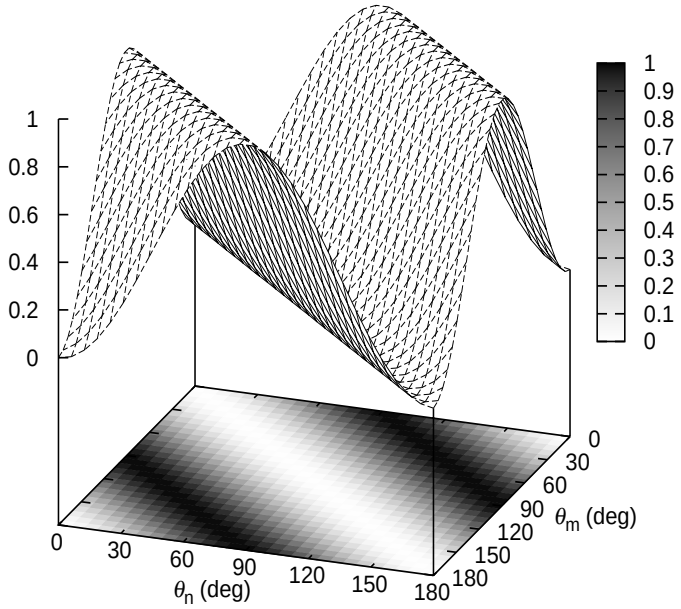

Figure 2. Surface and contour plot of the dipole plane angular correlation function (19) for fixed-in-space H_2 molecules as a function of θ_n and θ_m. The molecules are aligned perpendicular to the electric field vector and the direction of propagation of the incoming radiation.

Function (19) is exactly the same as obtained in [10], and it produces the identical result if the angle θ_m takes values between $[-\pi, 0]$ as in [10]. However, with the use of the usual definition of polar angles θ_n and θ_m running in between $[0, \pi]$, our result leads to different interpretation of the ACF (19). According to figure 2 the zero line of the ACF is along the $\theta_n = \theta_m$ diagonal, and not on the $\theta_m = \pi - \theta_n$ diagonal as suggested in [10].

In order to show how the interference influences the ACF (18), figure 3 depicts the two-photon ACF computed for the same case without accounting for the interference. This means, that the four components of the first term of (18) are summed up incoherently. Comparing figures 2 and 3 one can see that the interference has the

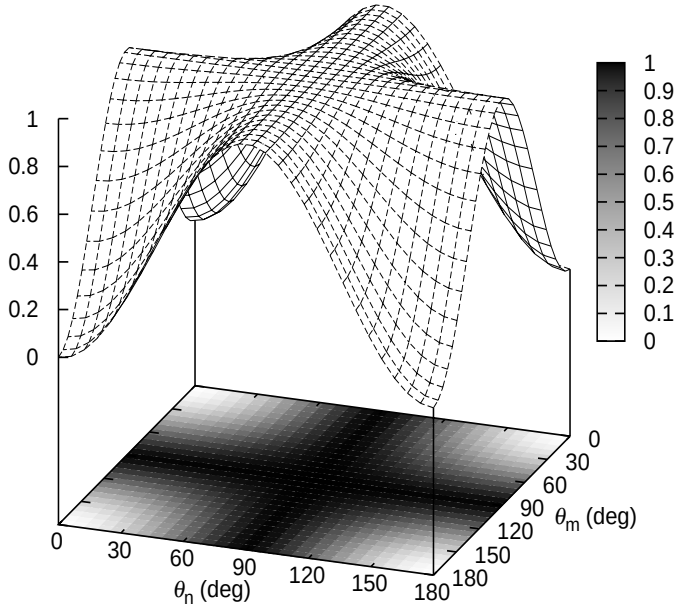

Figure 3. Surface and contour plot of the dipole plane angular correlation function of fixed-in-space H_2 molecules computed without interference. The molecules are aligned perpendicular to the electric field vector and direction of propagation of the incoming radiation.

strongest influence along the diagonals and no influence at the sides, if one detector is aligned parallel to the polarization vector of the incident light ($\theta_{n/m} = 0^\circ$ or 180°). In these cases, a single cut from the surface has a clear nonconstant shape, but it is not due to the interference. On the other hand, figures 2 and 3 indicate that the zero diagonal in figure 2 is due to complete destructive interference. If one needs to study interference experimentally in the discussed case by taking a single cut from the surface with one detector fixed, it should be placed preferably perpendicular to the electric field vector of the linearly polarized incident radiation.

3.2. Randomly oriented H_2 and polarization insensitive detectors

We may simplify (9) assuming that the radial parts of the dipole transition matrix elements are independent of J, and using, that for the initial and final states of the process $\Omega_i = \Omega_f = 0$. Summations over J_m and J_n can be carried out by applying (A.3) twice, and the sum over J_f using the orthogonality of the $3j$ symbols. Equation (9) is then reduced to the form

$$\frac{\mathrm{d}\sigma^2_{nm}}{\mathrm{d}\Omega_n \mathrm{d}\Omega_m} = \frac{\alpha^4 \omega_i \omega_n^3 \omega_m^3}{4\pi^2 c^3} \chi^{\mathrm{diss}} \sum_{K'Q'} \hat{K}'^2 \left| \Gamma^{-1} \sum_K F^{Q'}_{KK'} \sum_{\Omega_n \Omega_m} (-1)^{K-\Omega_m-2\Omega_n} \langle \nu_n, r_0 | \nu_i, r_0 \rangle \times \right.$$
$$\begin{pmatrix} 1 & 1 & K \\ \Omega_m - \Omega_n & \Omega_n & -\Omega_m \end{pmatrix} \begin{pmatrix} K & 1 & K' \\ \Omega_m & -\Omega_m & 0 \end{pmatrix} \times$$
$$\left. \langle \Omega_f | T^{(1)}_{q_m} | \Omega_m \rangle \langle \Omega_m | T^{(1)}_{q_n} | \Omega_n \rangle \langle \Omega_n | T^{(1)}_{q_i} | \Omega_i \rangle \right|^2 . \qquad (20)$$

Performing summations over K, K', Ω_n and Ω_m, and simplifying the dipole transition matrix elements as discussed in the previous section, the ACF takes the form similar to (18). Now, however, the information about all photons (including incident radiation) is expressed by the $F^{Q'}_{KK'}$ terms

$$f(\theta_n, \phi_n, \theta_m, \phi_m) = \sum_{Q'} 3|\frac{2}{3}F^{Q'}_{01} - \frac{1}{3}F^{Q'}_{11} + \frac{1}{15}F^{Q'}_{21}|^2 + \sum_{Q'} 7|\frac{2}{5}\sqrt{\frac{2}{7}}F^{Q'}_{23}|^2. \tag{21}$$

The form of equation (21) is independent of the coordinate system, polarization of the incident light and polarization sensitivities of the detectors. Only $K' = 1, 3$ values remain, which can be interpreted as follows. In the molecular frame the process leads to an emission of one linearly and one circularly polarized photon. The fact that the first photon may be linearly or circularly polarized in the molecular frame is reflected in the interference between the $F^{Q'}_{K1}$ terms. Only one $F^{Q'}_{K3}$ component is presented because $K = 2$ and $K' = 3$ is the only combination allowed by the triangular conditions in the dipole approximation for $K' = 3$. All experimentally observable results presented below can be obtained from (21), or equally from (11) by integrating over the molecular orientations.

3.2.1. Linearly polarized incident light The case of linearly polarized incident light was treated in the geometry illustrated in figure 1. Inserting explicit values of the $F^{Q'}_{KK'}$ given via (10) in (21), the ACF takes form

$$f(\theta_n, \phi_n, \theta_m, \phi_m) = \frac{1}{328\pi^4}(19|\epsilon^n_0\epsilon^m_1 + \epsilon^n_1\epsilon^m_0|^2 + 19|\epsilon^n_0\epsilon^m_{-1} + \epsilon^n_{-1}\epsilon^m_0|^2 + 8|\epsilon^n_1\epsilon^m_1|^2 + 8|\epsilon^n_{-1}\epsilon^m_{-1}|^2 + 8|2\epsilon^n_0\epsilon^m_0 + \epsilon^n_{-1}\epsilon^m_1 + \epsilon^n_1\epsilon^m_{-1}|^2). \tag{22}$$

Comparison of (22) and (18) shows that, if the molecular sample is randomly oriented, $\epsilon^n_j\epsilon^m_j$ and $\epsilon^n_j\epsilon^m_{-j}$ components are present in the ACF, which are absent for the special orientation discussed in the previous section. In addition, we note that the summation over M_i and M_f smears out the interference between $\epsilon^n_0\epsilon^m_1 + \epsilon^n_1\epsilon^m_0$ and $\epsilon^n_0\epsilon^m_{-1} + \epsilon^n_{-1}\epsilon^m_0$ terms. The analytic form of the ACF (22) can be calculated inserting components (15) to (22), and integrating over the polarization sensitivities of the detectors. The normalized ACF then takes the form

$$f(\theta_n, \pi/2, \theta_m 3\pi/2) = \frac{1}{164}(111 - 25(\cos 2\theta_m + \cos 2\theta_n) + 3\cos 2(\theta_m + \theta_n)), \tag{23}$$

which is depicted in figure 4.

The surface plotted in figure 4 shows that the shape of the ACF for the special orientation plotted in figure 2 is mostly smeared out. However, the ACF exhibits still a clear dependence on the emission angles, which can be verified experimentally. One may see that in contrast to the fixed-in-space case, the highest coincidence probability is obtained when the two detectors are facing each other perpendicular to the electric field vector of the incident light. The function in figure 4 resembles somehow the ACF from [10] weighted with initial excitation probability of $\sin^2\theta$ (see, figure 4a' in [10]). Clear differences can be still pointed out. The present ACF has a clear isotropic background

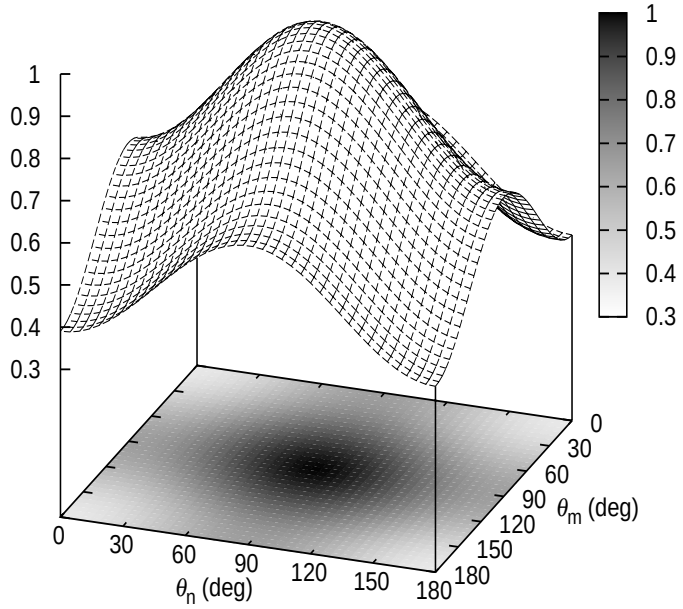

Figure 4. Surface and contour plot of the dipole plane angular correlation function (23) for randomly oriented H_2 molecules excited by linearly polarized radiation.

and the double peak structure obtained in [10] is missing. The background in the present calculations explains, without invoking finite opening angles of the detectors, why the photon-photon coincidences were observed in [9] despite the experimental geometry was set to a zero point of the ACF computed in [10].

In order to analyze the ACF (22) in more detail, figure 5 depicts three functions summed in figure 4. The uppermost panel of figure 4 shows the contribution from the first two terms in (22), the middle panel shows the contribution from the third, and fourth terms, and the lowermost panel the fifth term. The first and second, as well as third and fourth terms were summed because they result in equal dependencies, respectively. The function shown in the uppermost panel of figure 5 for a random orientation is the same as in figure 4a' in [10] (but rotated by 90° around the vertical axis piercing the horizontal plane at $\theta_n = \theta_m = 90°$, which is due to different definitions of spherical angle θ discussed above). Additional investigations showed that the ACF derived in [10] and averaged with $\sin^2\theta$ does not reproduce the full solution of the problem for randomly oriented molecules. We assume that this is because rotation of the two-photon state obtained from the second-order correlation function does not produce $\epsilon_j^n \epsilon_j^m$ and $\epsilon_j^n \epsilon_{-j}^m$ components. Therefore, the approximate approach in [10] gives only a part of the full solution (22). We emphasize that the angular conservation requires that $|q_i| = |q_n + q_m| = 1$ holds always in the molecular frame, and it is the transformation to the laboratory frame which produces the additional terms in (22). From figure 5 we also see that the linear combination of the three parts does not always have to be symmetric for the two diagonals. It is by chance that the sum is symmetric in the case of linearly polarized light shown in figure 4.

Results of the present calculations of the ACF are compared to the experimental

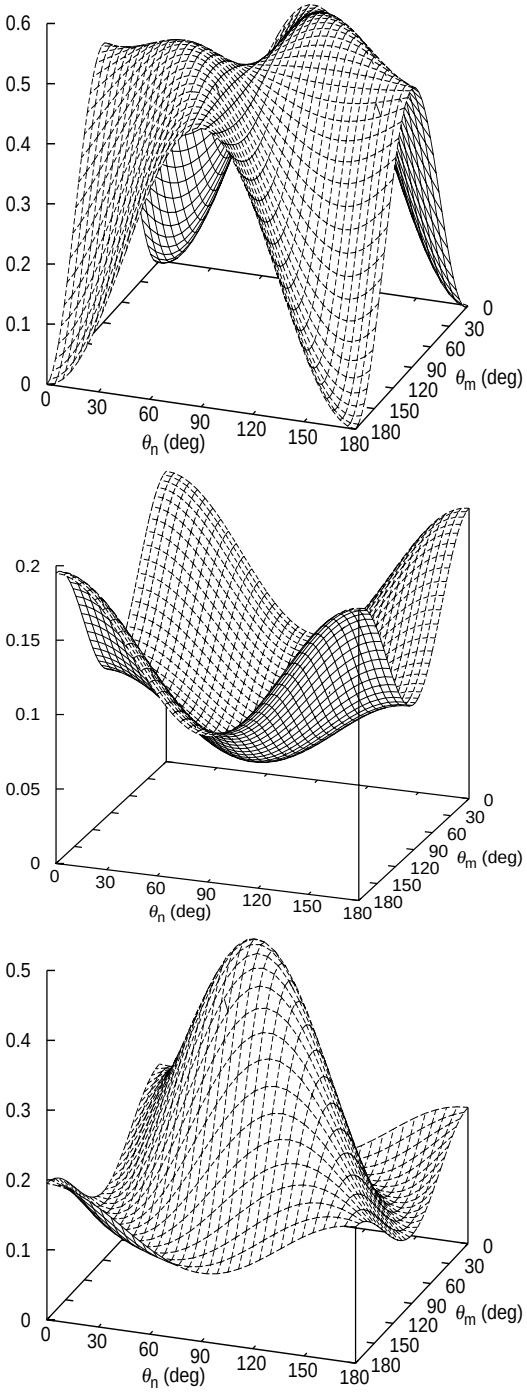

Figure 5. Surface plots of the three different functions summed in equation (22). Uppermost panel: Function obtained from the first two terms. Middle panel: Function obtained from the third and fourth term. Lowermost panel: Function obtained from the fifth term. The scales show the relative contributions of these functions to the ACF (22) shown in figure 4.

[16] and theoretical [10] ones in figure 6. The figure shows a cut from the surface depicted in figure 4 along the $\theta_n = \pi - \theta_m$ diagonal. As one can see, the coincidence rate function computed in [10] has a minimum and vanishes at $\theta_m = 0°$ (dashed curve).

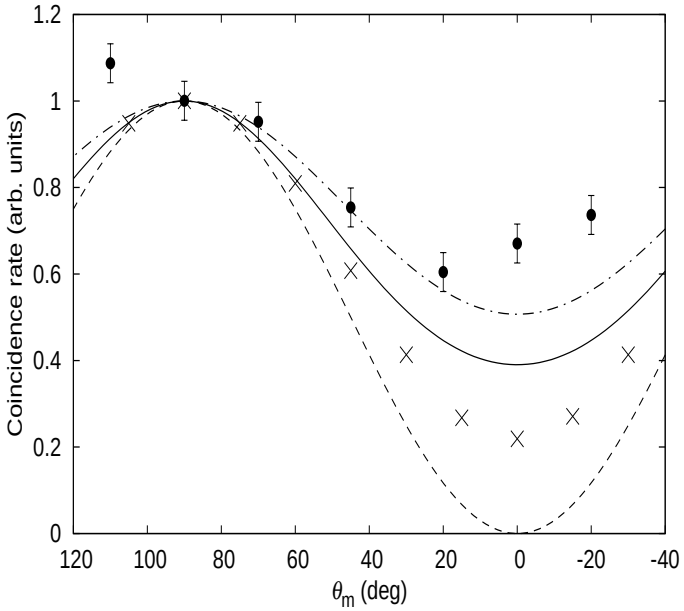

Figure 6. Single cut of the dipole plane two-photon ACF for randomly oriented H_2 molecule excited by linearly polarized incident light. The detectors are facing each other with relation $\theta_n = \pi - \theta_m$. Dots: Experimental data from [16]. Solid line: Present calculation. Dash-dotted line: Present calculation convolved with the detector opening angles 0.64 sr used in [16]. Dashed line: Calculation [10]. Crosses: Calculation [10] convolved with the detector opening angles 0.64 sr. All results are normalized to the unity at $\theta_m = 90°$.

The minimum in the experimental coincidence rate [16] (dots) is, however, not so deep, even if one accounts for the finite detector opening angles in the theory (crosses). This disagreement was explained in [16] by the large pressure effect. It was suggested in [16] that experimental data may saturate to the theoretical predictions (crosses) with decreasing of pressure. One can see from figure 6, that the presently computed coincidence rate (solid curve) has the same shape but a smaller dip in the minimum around $\theta_m = 0°$. Due to the constant background in the presently computed ACF (22), the rate for detecting both photons parallel to the polarization vector of the incident light has a limit of about 0.4 (not zero as suggested in [10]). The finite detector opening angles used in [16] additionally enlarges the coincidence rate around $\theta_m = 0°$ (dash-dotted curve). Thus, we may conclude that the lower pressure of 0.13 Pa of the H_2 sample used in [16] approaches already the limit where collisions do not considerably destroy the entanglement in the system. Slight asymmetry of the experimental ACF [16] and its disagreement with the presently computed ACF (dash-dotted curve) at $\theta_m = 110°$, $0°$ and $-20°$ might be due to entangled atom-pair reactions suggested in [16].

As a final remark, we note that the linear dichroism pattern [33], defined as the difference between the ACF recorded with the incident light polarization along the y-axis and the ACF with the incident light polarized along the z-axis, has the same shape as the function shown in figure 4. The only difference is that the linear dichroism function

takes values between about (-0.4,0.4). This is a direct consequence of the symmetry and periodicity of function (23).

3.2.2. Circularly polarized incident light The most convenient form of the ACF in the case of circularly polarized incident light is obtained when the incoming light is chosen to propagate along the z-axis in the laboratory frame (see figure 1). By inserting the components of the right-handed circularly polarized incident light into (21), we obtain

$$f(\theta_n,\phi_n,\theta_m,\phi_m) = \frac{1}{76\pi^4}(\frac{8}{3}|\epsilon_0^n\epsilon_1^m + \epsilon_1^n\epsilon_0^m|^2 + 5|\epsilon_0^n\epsilon_{-1}^m - \epsilon_{-1}^n\epsilon_0^m|^2 + 8|\epsilon_1^n\epsilon_1^m|^2 + \frac{52}{3}|\epsilon_{-1}^n\epsilon_{-1}^m|^2 + |2\epsilon_0^n\epsilon_0^m + \epsilon_{-1}^n\epsilon_1^m + \epsilon_1^n\epsilon_{-1}^m|^2). \quad (24)$$

The left-handed circularly polarized case can be described by exchanging simultaneously the numerical prefactors of the first and second terms, and third and fourth terms. Note, that the function (24) has the same terms as in (22), but with different weights, which are not symmetric for the first and the second, and the third and the fourth terms. However, since the functions produced by these pairs are equal, as mentioned above, the total ACFs for right- and left-handed circularly polarized light are equal. This means that, even if the detectors are polarization sensitive, one cannot observe circular dichroism [33] in the two-photon ACF from H_2. The function (24) is explicitly given by

$$f(\pi/2,\phi_n,\pi/2,\phi_m) = \frac{1}{38}(37 + \cos 2(\phi_m - \phi_n)). \quad (25)$$

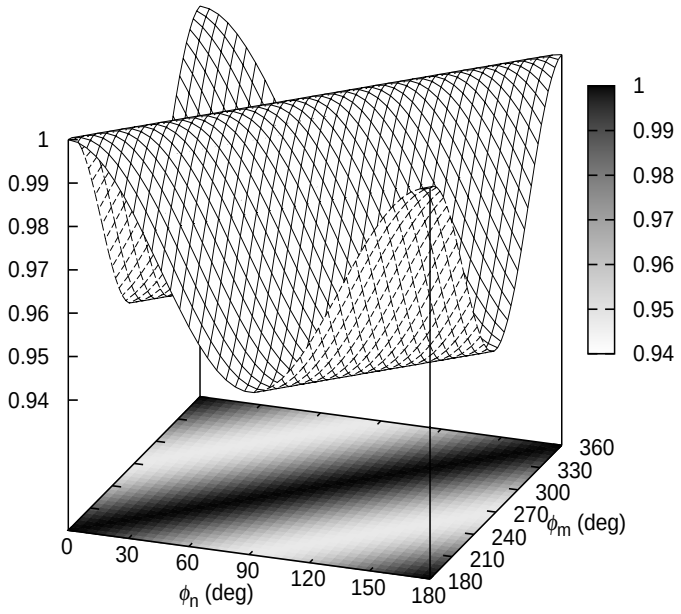

Figure 7. Surface and contour plot of the dipole plane angular correlation function (25) for randomly oriented H_2 molecules excited by circularly polarized light.

Figure 7 shows the two-photon ACF (25) for randomly oriented molecules excited by circularly polarized incident light. One can see that the ACF in this case is almost constant and does not change by more than 5 %. The figure also shows that the

maximum of the function corresponds to the $\phi_m = \pi + \phi_n$ diagonal. This result is expected and physically meaningful because, if the incident light is circularly polarized, there is no preferred direction in the dipole plane when both detectors are facing each other. We can also conclude that, in contrast to the case of linearly polarized light, the function in figure 7 has additional maxima in the two corners, where the photons are detected in the same direction.

3.3. Randomly oriented H_2 and polarization sensitive detectors

As an example of an ACF measured by polarization sensitive detectors, the case of molecules excited by linearly polarized light is studied. The two photons are counted by detectors sensitive to linear and circular polarization, such that detector sensitive to the linear polarization is at the direction θ_n. Selecting the detector at θ_n to be sensitive to linear polarization parallel ($\|$) or perpendicular ($\perp$) to the direction of propagation of the incident light, we obtain from (22) two functions

$$f_{\|}(\theta_n, \pi/2, \theta_m, 3\pi/2) = \frac{1}{102}(64 - 10\cos 2\theta_m - 25\cos 2\theta_n + 3\cos 2(\theta_m + \theta_n)) \tag{26}$$

$$f_{\perp}(\theta_n, \pi/2, \theta_m, 3\pi/2) = \frac{1}{62}(47 - 15\cos 2\theta_m). \tag{27}$$

The choice of the sensitivity between left- and right-handed circular polarization of the detector at θ_m do not alter the above functions.

The functions (26) and (27) are plotted in the upper and lower panels of figure 8, respectively. The function in the lower panel shows that the ACF is independent of the emission angle of the linearly polarized light which is perpendicular to the direction of propagation of the incident radiation. On can also see that the coincidence detection is most probable if the circularly polarized photon is detected perpendicular to the electric field vector of the incoming radiation ($\theta_m = 90°$). On the other hand, the upper panel of figure 8 shows clear variations as a function of both angles. We note that the sides of the surface are slightly asymmetric. As an example, the coincidence detection is a bit more probable, if the detector sensitive to the linearly polarized photon is in the perpendicular direction of the electric field vector of the incoming light $\theta_n = 90°$ and $\theta_m = 0°$, than if the detector sensitive to circular polarization is in the corresponding direction $\theta_m = 90°$ and $\theta_n = 0°$. This behaviour was indicated already by analysis of the lowermost panel of figure 8, since functions (26) and (27) do not depend on the detector sensitivity to the direction of polarization of the circularly polarized photons. Therefore, if functions (26) and (27) are summed before normalization one obtains a function, which is proportional to the case of polarization insensitive detectors (23).

As a final example, the two-photon coincidence probability as a function of the angle of linear polarization sensitivity ξ_n is shown in figure 9 for two special geometries (see caption of figure 9). For both geometries we obtained that the coincidence detection probability show clear measurable variations as a function of ξ_n. One can see that the two cases show opposite behaviour. If the linearly polarized photon is detected parallel to the electric field vector of the incident light, the maximal coincidence rate corresponds

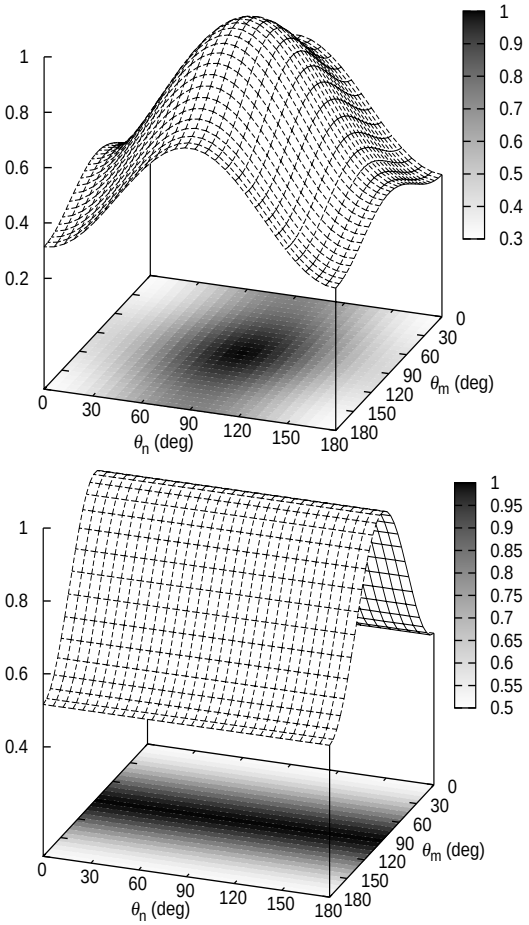

Figure 8. Surface and contour plots of the dipole plane two-photon ACF detected by polarization sensitive detectors. The H_2 molecules are randomly oriented and excited by linearly polarized light. Upper panel: The detector on the θ_n direction is sensitive to the linear polarization parallel to the direction of propagation of the incident light. Lower panel: The detector on the θ_n direction is sensitive to linear polarization perpendicular to the direction of propagation of the incident light. Detector on the θ_m direction in both cases is sensitive to the left- or right-handed circular polarization.

to the detection of the photons polarized parallel to the direction of propagation of the incident light. On the other hand, if the linearly polarized photons are detected in the direction perpendicular to the electric field vector of the incident radiation, the maximal coincidence rate corresponds to the detector sensitive to photons polarized perpendicular to the direction of propagation of the incident light.

4. Conclusion

We have provided a general theoretical framework to simulate the double differential cross section and ACF of two photons emitted by two entangled atomic fragments after neutral (pre)dissociation of a superexcited diatomic molecule. The theory can be applied to the studies of fixed-in-space and randomly oriented molecules with

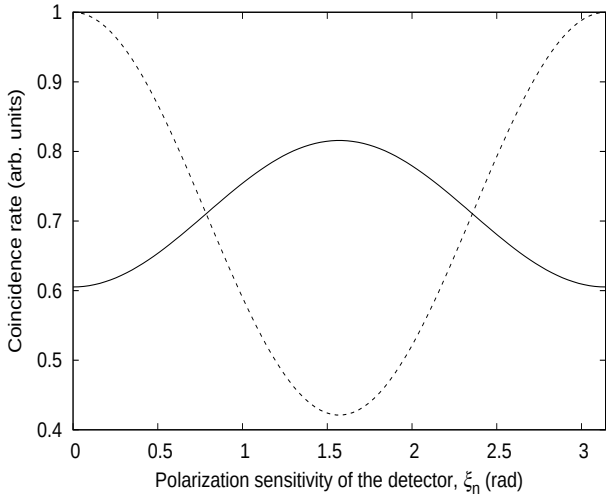

Figure 9. Coincidence intensity obtained in the dipole plane by detectors sensitive to circular and linear polarization as a function of the linear polarization angle ξ_n in two orientations. Dashed line: The detector sensitive to the linear polarization is parallel ($\theta_n = 0°$) and the detector sensitive to the circular polarization is perpendicular to the electric field vector of the incident light ($\theta_m = 90°$). Solid line: The detector sensitive to the linear polarization is perpendicular ($\theta_n = 90°$) and detector sensitive to the circular polarization is parallel ($\theta_m = 0°$) to the electric vector of the incident light.

different polarizations of the incoming light and polarization sensitivities of the photon counters. The presented model was used to calculate the analytical forms of the ACF of two photons following the dissociation of the $Q_2\,{}^1\Pi_u(1)$ superexcited state of H_2 in different cases. In the case of a fixed-in-space H_2 molecule, we demonstrated how the interference influences the two-photon ACF. In the case of randomly oriented molecules and polarization insensitive detectors, the two-photon ACFs induced by linearly and circularly polarized incident light were obtained. The present theory provides more complete description of the process than the previously published calculations [10] and it agrees with the recent experimental data [16] considerably better. It was shown that in the studied case, the linear dichroism pattern has the same shape as ACF obtained by using horizontally polarized incident light, and that there is no circular dichroism in the ACF. In the case of polarization sensitive detectors we obtained that the shape of ACF depends strongly on the linear polarization angle of the detected photon, but shows no difference between detector sensitivity to the left- and right-handed circular polarization.

Acknowledgments

K J would like to acknowledge the Finnish Academy for financial support under research grant Nr. 125480. Ph V D gratefully acknowledge the Marie Curie fellowship (PIIF-GA-2008-219224) by the European Commission.

Appendix

In the following we list some identities utilized in the present derivation. The analytical integration over the rotational parts of the wave functions is well known and can be found e.g. in [22]. The matrix elements are

$$\langle JM\Omega|D^{(k)*}_{pq}(\omega)|J'M'\Omega'\rangle = \hat{J}\hat{J}'(-1)^{M-\Omega}\begin{pmatrix} J & k & J' \\ -M & p & M' \end{pmatrix}\begin{pmatrix} J & k & J' \\ -\Omega & q & \Omega' \end{pmatrix}, \tag{A.1}$$

where index p refers to the laboratory coordinates and q to the molecular frame.

Summation over M_m and M_n in (9) can be carried out analytically with the aid of (2.19) of Rotenberg *et al* [34]. In our case it reads:

$$\sum_{KQ}\hat{K}^2(-1)^{J+J_d+J'+k_1+k_2+K-M+q_2}\begin{pmatrix} J & K & J' \\ -M & -Q & M' \end{pmatrix}\begin{pmatrix} k_1 & k_2 & K \\ q_1 & q_2 & Q \end{pmatrix}\begin{Bmatrix} k_1 & k_2 & K \\ J' & J & J_d \end{Bmatrix}$$
$$= \sum_{M_d}\begin{pmatrix} J & k_1 & J_d \\ -M & q_1 & M_d \end{pmatrix}\begin{pmatrix} J_d & k_2 & J' \\ -M_d & q_2 & M' \end{pmatrix}. \tag{A.2}$$

Summation over J_n and J_m in (20) was carried out using (4.16) from Zare [35], which in our case reads:

$$\sum_{J_d}\hat{J}_d^{\,2}(-1)^{J_d}\begin{Bmatrix} k_1 & k_2 & K \\ J' & J & J_d \end{Bmatrix}\begin{pmatrix} J & k_1 & J_d \\ -\Omega & q_1 & \Omega_d \end{pmatrix}\begin{pmatrix} J_d & k_2 & J' \\ -\Omega_d & q_2 & \Omega' \end{pmatrix}$$
$$= (-1)^{K-k_1-k_2-J'-J+q_1+\Omega'}\begin{pmatrix} k_1 & k_2 & K \\ q_1 & q_2 & -(q_1+q_2) \end{pmatrix}\begin{pmatrix} J & K & J' \\ -\Omega & \Omega'-\Omega & \Omega' \end{pmatrix}. \tag{A.3}$$

References

[1] Kouchi N, Ukai M and Hatano Y 1997 *J. Phys. B: At. Mol. Opt. Phys.* **30** 2319
[2] Hatano Y 2001 *J. Electron Spectrosc. Relat. Phenom.* **119** 107
[3] Hiyama M, Kosugi N and Nakamura H 1997 *J. Chem. Phys.* **107** 9370
[4] Platzman R L 1962 *Radiat. Res.* **17** 419; *Vortex* **23** 372
[5] Latimer C J, Irvine A D, McDonald M A and Savage O G 1992 *J. Phys. B: At. Mol. Opt. Phys.* **25** L211
[6] Odagiri T, Uemura N, Koyama K, Ukai M, Kouchi N and Hatano Y 1995 *J. Phys. B: At. Mol. Opt. Phys.* **28** L465
[7] Glass-Maujean M, Klumpp S, Werner L, Ehresmann A and Schmoranzer H 2004 *J. Phys. B: At. Mol. Opt. Phys.* **37** 2677
[8] Arai S, Kamosaki T, Ukai H, Shinsaka K, Hatano Y, Ito Y, Koizumi H, Yagishita A, Ito K and Tanaka K 1988 *J. Chem. Phys.* **88** 3016
[9] Odagiri T, Murata M, Kato M and Kouchi N 2004 *J. Phys. B: At. Mol. Opt. Phys.* **37** 3909
[10] Miyagi H, Ichimura A and Kouchi N 2007 *J. Phys. B: At. Mol. Opt. Phys.* **40** 617
[11] Ryan S R, Czuchlewski S J and McCusker M V 1977 *Phys. Rev.* A **16** 1892
[12] Murata M, Odagiri T and Kouchi N 2005 *J. Electron Spectrosc. Relat. Phenom.* **144-147** 147
[13] Murata M, Odagiri T and Kouchi N 2006 *J. Phys. B: At. Mol. Opt. Phys.* **39** 1285
[14] Odagiri T, Miyagi H, Murata M, Fukuzawa H, Kurokawa M, Kitajama M and Kouchi N 2009 *J. Phys. B: At. Mol. Opt. Phys.* **42** 055101

[15] Odagiri T, Funatsu K, Tanabe T, Suzuki I O, Kitajima M and Kouchi N 2009 *J. Phys. B: At. Mol. Opt. Phys.* **42** 225101
[16] Tanabe T, Odagiri T, Nakano M, Suzuki I H and Kouchi N 2009 *Phys. Rev. Lett.* **103** 173002
[17] Guberman S L 1983 *J. Chem. Phys.* **78** 1404
[18] Bottcher C 1974 *J. Phys. B: At. Mol. Opt. Phys.* **7** L352
[19] Borges I and Bielschowsy C E 2001 *Chem. Phys. Lett.* **342** 411
[20] Borges I and Bielschowsy C E 2000 *J. Phys. B: At. Mol. Opt. Phys.* **33** 1713
[21] Lefebvre-Brion H and Field R W 2004 *The Spectra and Dynamics of Diatomic Molecules* (Amsterdam: Elsevier)
[22] Brown J M and Carrington A 2003 *Rotational Spectroscopy of Diatomic Molecules* (Cambridge: Campridge University Press)
[23] Singer S J, Freed K F and Band Y B 1984 *J. Chem. Phys.* **81** 3064
[24] Band Y B and Freed K F 1981 *Chem. Phys. Lett.* **79** 238
[25] Vigué J, Beswick J A and Broyer M 1983 *J. Physique* **44** 1225
[26] Singer S J and Freed K F 1983 *J. Chem. Phys.* **79** 6060
[27] Mukamel S and Jortner J 1974 *J. Chem. Phys.* **61** 5348
[28] Glass-Maujean M and Beswick J A 1989 *J. Chem. Soc., Faraday Trans.* **85** 983
[29] van Brunt R J and Zare R N 1968 *J. Chem. Phys.* **48** 4304
[30] Blum K and Kleinpoppen H 1979 *Phys. Rep.* **52** 203
[31] Edmonds A R 1960 *Angular Momentum in Quantum Mechanics* (Princeton: Princeton University Press)
[32] Wang J B, Stelbovics A T and Williams J F 1994 *Z. Phys. D* **30** 119
[33] Rodger A and Nordenń B 1997 *Circular Dichroism and Linear Dichroism* (Oxford: Oxford University Press)
[34] Rotenberg M, Bevins R, Metropolis N and Wooten J K Jr 1959 *The 3j- and 6-j Symbols* (Cambridge, Massachusetts: Massachusetts Institute of Technology Press)
[35] Zare R N 1988 *Angular Momentum* (New York: Wiley Interscience)